QUADRUPOLE LENSES

FOCUSING PROPERTIES
OF
QUADRUPOLE LENSES

by

DARIUS DOMAS SLAVINSKAS, B.A.Sc.

A Thesis

Submitted to the Faculty of Graduate Studies

in Partial Fulfilment of the Requirements

for the Degree

Master of Science

McMaster University

May 1963

MASTER OF SCIENCE (1963) McMASTER UNIVERSITY
Hamilton, Ontario.

TITLE: Focusing Properties of Quadrupole Lenses

AUTHOR: Darius Domas Slavinskas, B.A.Sc.

SUPERVISOR: Dr. T. J. Kennett

NUMBER OF PAGES: v, 48

SCOPE AND CONTENTS:

The properties of electrostatic quadrupole lenses are investigated both theoretically and experimentally. A method for measuring the effective lens length is developed and used. Previously reported (6) focusing equations for the two lens system provide an implicit solution involving trigonometric and hyperbolic functions. A nomograph was designed as an aid in carrying out this solution numerically. The two lens system was evaluated for various combinations of object distance, lens separation and image distance. Measured values of focal strengths were compared to theoretical values. Finally, measurements were made on the effective focal strength as a function of radial displacement from the central axis.

ACKNOWLEDGEMENTS

The author wishes to express grateful appreciation to his director of research Dr. T. J. Kennett for patient guidance and encouragements during moments of near despair. He is also indebted to Dr. G. L. Keech for his shown interest in this experiment accompanied by valuable suggestions.

TABLE OF CONTENTS

LIST OF DIAGRAMS

A. INTRODUCTION

During recent years quadrupole lenses have received considerable attention and have been found useful in high-energy accelerators (1, 6) and mass spectrometers (5, 7). One rewarding feature about them is the mathematical predictability of their properties, in contrast to the largely empirical nature of many other focusing devices. As lenses they are unique in that their properties lack cylindrical symmetry. They are converging in one plane but diverging in another. However, the property that the ion motion in one plane is independent of position in the other plane, contributes considerably to simplicity of mathematics involved. Ion motion in the converging plane is harmonic, since the restoring force is proportional to displacement from the central axis. In the diverging plane the force has same magnitude but opposite sense. Thus this motion is described by exponentials with real exponents (or hyperbolic sinusoids).

Due to the strong-focusing principle involved, it is possible to obtain an overall convergent effect with a number of equal strength alternately converging and diverging quadrupole lenses. A good example are two equal strength quadrupole lenses placed halfway between a point object and point image. Looking at one plane, one of the lenses would be converging and the other diverging. In fact, when the two lenses are placed off the center, there is a plane in which the diverging lens is stronger, but the overall effect is still convergent.

This thesis is divided into two main parts - theoretical and experimental. The theory is included to supply the necessary background and to provide formulae which were vital to the experimental techniques employed. Comparisons were made between theoretically predicted and experimentally observed results.

B. THEORY

1. The Quadrupole Lens

The properties of electric and magnetic quadrupole lenses have been discussed by various writers (1 to 8). In this thesis only electrostatic lenses are considered.

Ideally, the equipotential lines of a quadrupole lens should form a family of rectangular hyperbolae. In practice, this field can be well approximated (Giese (7)) by the use of four circular cylinders. Such a lens is shown in fig. 1, where cylinders have radii 1.25 R and the separation between cylinders (or the aperture) is 2R. The rectangular hyperbolae with intercepts at $y = \pm R$ and $z = \pm R$ have a radius of curvature R at their vertexes and larger radii off to the sides. The value of 1.25R, used for the cylinder radius in this experiment, is an acceptable compromise between the different hyperbolae radii (Giese (7), Dayton et al (4)). As shown in fig. 1, each cylinder is held at a voltage $+V_o$ or $-V_o$.

Assuming an ideal lens, the equipotential surfaces inside it are given by

$$V = G(y^2 - z^2).$$

Since $V = V_o$ at $z=0$ and $y = \pm R$, we have $G = V_o/R^2$, and hence

$$V = \frac{V_o}{R^2}(y^2 - z^2). \qquad (1)$$

Differential equations can now be written for the motion of a positive ion of charge ne and mass m.

$$\frac{d^2y}{dt^2} = -\frac{ne}{m}\frac{\partial V}{\partial y} = -\frac{n2eV_o}{mR^2}\,y \tag{2}$$

and

$$\frac{d^2z}{dt^2} = -\frac{ne}{m}\frac{\partial V}{\partial z} = \frac{n2eV_o}{mR^2}\,z \quad . \tag{3}$$

Their solution is given by

$$y = A\cos(\omega t + \phi) \tag{4}$$

and

$$z = B\cosh(\omega t + \theta_1)$$

or

$$z = C\sinh(\omega t + \theta_2) \quad , \tag{5}$$

where

$$\omega^2 = \frac{2neV_o}{mR^2} \quad . \tag{6}$$

Two equations are written for z, since one hyperbolic function is insufficient to satisfy all possible initial conditions. Assume now that the ion enters the lens with a velocity component v_x in the x-direction. In the nonrelativistic case we can write

$$v_x = \sqrt{\frac{2E}{m}} = \sqrt{\frac{2neV_s}{m}} \quad ,$$

where V_s is the voltage through which the ion was accelerated. Hence,

$$t = \frac{x}{v_x} = x\sqrt{\frac{m}{2neV_s}} \quad . \tag{7}$$

Substitution of expressions (6) and (7) in equations (4) and (5) results in the following ion path equations:

$$y = A\cos(kx + \phi) \tag{8}$$

and $z = B \cosh (kx + \theta_1)$

or $z = C \sinh (kx + \theta_2)$, } (9)

where $k = \frac{1}{R}\sqrt{\frac{V_o}{V_s}}$. (10)

It is seen from equations (8) and (9) that the ions will converge in one plane and diverge in the other. For the lens shown in fig. 1, positive ions will converge in the y-X plane and diverge in the z-x plane. For negative ions, or electrons, the roles of convergence and divergence are simply interchanged. The parameter k has units of inverse distance and will be referred to as the wave number. In the relativistic case equations (8) and (9) remain unchanged but k has a different definition. According to Enge (6), the relativistic wave number is given by

$$k = \frac{1}{R}\sqrt{\frac{nV_o}{E}} , \qquad (10a)$$

where $E = p\beta c/2$, in electron volts.

Although the physical length of lens shown in fig. 1 is ℓ_p, the effective length, ℓ , can be expected to be larger on account of fringe fields. Enge (6) gives the formula:

$$\ell = \ell_p + 2Rf , \qquad (11)$$

where f is a factor dependent on design and is expected to be less than unity. The quantity $k\ell$ is dimensionless and will be called the focal strength of the lens.

2. Focusing by One Lens

A lens, convergent in the y-x plane, is shown in fig. 2. The object, a point source, is at a distance a from the lens. Due to divergence in the z-x plane, the image will not be a point, but a line perpendicular to the paper. The "end view" of this image line is shown at a distance b from the lens. A solution for k in terms of a, b and ℓ is given below.

Inside the lens, the ion (or electron) path is given by equation (8), i.e.:

$$y = A \cos (kx + \phi). \tag{12}$$

Since the path in region $-a \leq x \leq 0$ is a straight line, we can impose the boundary condition

$$a \left.\frac{dy}{dx}\right|_{x=0} = \left. y \right|_{x=o}, \tag{13}$$

which results in

$$\tan \phi = -\frac{1}{ka}. \tag{14}$$

Similarly, at $x = \ell$ we have

$$\tan (k\ell + \phi) = \frac{1}{kb}. \tag{15}$$

Combining equations (14) and (15) will eventually result in

$$\tan k\ell = \frac{k(a+b)}{k^2ab-1} \tag{16}$$

This last expression is the implicit solution for k we set out to obtain. The solution for a collimated beam source is obtained by simply letting a approach infinity in equation (16). Thus,

$$\tan k_\infty \ell = \frac{1}{k_\infty b} \quad . \tag{17}$$

3. Focusing by Two Lenses

With two lenses it is possible to focus a point source to a point image. Likewise, a collimated beam can be focused to a point image on the x-axis. The physical arrangement of the focusing system is shown in fig. 3, where

a is the object distance,

b is the image distance,

ℓ is the effective lens length,

s is the lens separation,

k_1 and k_2 are the wave numbers of first and second lens respectively.

Note that in the plane shown by fig. 3 (the y-x plane) the first lens is diverging and the second lens is converging. The reverse is true, of course, in the z-x plane. It is required to solve for k_1 and k_2 in terms of the other parameters. A solution was given by Enge (6) in milepost form. The following is a reproduction of that solution with an attempt to fill in some of the remaining landscape.

Consider the y-x plane (as in fig. 3). Since the first lens is diverging, the equation of motion inside it will be given by a hyperbolic function, such as expressions (9). We have two possible choices - a hyperbolic cosine or a hyperbolic sine. Let us

choose the hyperbolic cosine first and write

$$y = A \cosh\left[k_1(x-a) + \phi_1\right] . \tag{18}$$

Applying boundary condition (13) at position I (x=a) results in

$$\tanh \phi_1 = \frac{1}{k_1 a} . \tag{19}$$

Since $\tanh \phi_1 \leq 1$, this boundary condition can be satisfied only when $k_1 a \geq 1$. In the case where $k_1 a < 1$, one must use the other hyperbolic function

$$y = A \sinh\left[k_1(x-a) + \phi_1'\right] . \tag{20}$$

The same boundary condition becomes now

$$\coth \phi_1' = \frac{1}{k_1 a} . \tag{21}$$

In this experiment all values of $k_1 a$ were greater than unity. Equation (20) will therefore not be further considered.

The second lens is converging. Hence the equation of motion inside it is given by a sinusoid,

$$y = B \cos\left[k_2(x-a-s-2\ell) + \phi_2\right] . \tag{22}$$

If we impose the boundary condition at position IV, we obtain

$$\tan \phi_2 = \frac{1}{k_2 b} . \tag{23}$$

Now there remain two as yet unapplied conditions. Firstly, the slope of ion path at the exit of the first lens (position II) is the same as the slope at the entrance of the second lens (position

III). Stated mathematically,

$$k_1 A \sinh(k_1\ell + \phi_1) = k_2 B \sinh(k_2\ell - \phi_2) . \qquad (24)$$

Secondly, the difference in values of y at III and II is equal to the slope at III multiplied by the separation s . In equation form we have

$$B\cos(k_2\ell - \phi_2) - A\cosh(k_1\ell + \phi_1) = sk_2B\sin(k_2\ell - \phi_2). \qquad (25)$$

Equations (24) and (25) can be combined to give

$$\frac{1}{k_1\ell}\coth(k_1\ell + \phi_1) = \frac{1}{k_2\ell}\cot(k_2\ell - \phi_2) - \frac{s}{\ell} . \qquad (26)$$

By similar arguments applied to the z-x plane one can obtain a second equation involving the unknowns k_1 and k_2 . However, time can be saved if we consider the point image as the object in the z-x plane. The situation then becomes entirely analogous to the previous one with values of k_1 and a exchanged by k_2 and b respectively. Thus a simple exchange of variables in (26) gives the second equation

$$\frac{1}{k_2\ell}\coth(k_2\ell + \theta_2) = \frac{1}{k_1\ell}\cot(k_1\ell - \theta_1) - \frac{s}{\ell} , \qquad (27)$$

where

$$\tan\theta_1 = \frac{1}{k_1 a} , \qquad (28)$$

and

$$\tanh\theta_2 = \frac{1}{k_2 b} . \qquad (29)$$

Expression (29) requires that $k_2 b$ be greater than unity. In all measurements of this experiment that condition was satisfied.

The wave numbers k_1 and k_2 are now implicitly determined by equations (26) and (27). For a collimated beam source a is allowed to approach infinity so that, in the limit, $\phi_1 = \theta_1 = 0$. Solution of these equations without some form of aid (such as a digital computer or specially designed charts) would be tedious to say the least. In view of this difficulty a nomograph (fig. 4) was constructed. Its detailed description is given in the following section.

4. Nomograph

The nomograph, shown in fig. 4, is an aid in determining focal strangths $k_1\ell$ and $k_2\ell$ for the two lens focusing system. It permits one to solve equations (26) and (27). The axis on the far left, labelled H, represents the hyperbolic term as a function of a/ℓ and $k_1\ell$ (or b/ℓ and $k_2\ell$). On the far right we have an axis labelled T, which represents the corresponding trigonometric term. The axis in the middle represents the lens separation s/ℓ. Values indicated by a straight-edge placed across all three axes will satisfy equations (26) and (27), i.e.:

$$H = T - s/\ell \ .$$

The procedure for finding $k_1\ell$ and $k_2\ell$ is as follows:

1.) Assume a number of values for $k_1\ell$. Mark the corresponding hyperbolic term values on the H-axis (using the given a/ℓ).

2.) Transfer these points to the T-axis by means of a straight-edge going through the given s/ℓ.

3.) Using the points on the T-axis and the known b/ℓ, find the corresponding values of $k_2\ell$. We are now able to plot a graph of $k_2\ell$ versus $k_1\ell$.

4.) The same procedure is now repeated starting with the T-axis and going to the H-axis. This results in a second plot of $k_2\ell$ versus $k_1\ell$. The point of intersection gives the solution.

This explanation is made somewhat lengthy for the sake of clarity. The actual process of using the nomograph is quite rapid. Error in values obtained for the focal strengths was found to be less than 0.5%.

C. EXPERIMENT

1. Description of Apparatus

(i) General

The general arrangement of apparatus is shown schematically in fig. 5. Focusing was carried out inside a brass tube of 5 foot (152.4 cm.) length and 2 7/8 inch inner diameter. Two quadrupole lenses were mounted on steel key-ways extending the whole length of the tube. The position of lenses could be adjusted without opening the vacuum system by means of hollow rods attached to the lenses which passed through rubber o-rings. Leads passed inside the hollow rods provided voltages to the lens poles.

The electron source (described later in more detail) was mounted on the sealing cap at the left end of the tube. The right end of the tube was terminated by the horn and screen of a "Tektronix" cathode ray tube. This arrangement permitted visual observation of image patterns.

A mechanical rotor pump and oil diffusion pump were used in series to provide the necessary vacuum. Pressure down to 4×10^{-6} mm. Hg. were obtained as measured by an ionization gauge. However, with the source in operation, the pressures increased by about one order of magnitude. Scattering of electrons on their way to the target screen will depend on their mean free path at the working pressure (about 5×10^{-5} mm. Hg.). According to Sears (9), the electron mean free path is given by

$$\lambda = \frac{4}{\sigma n} ,$$

where σ is the gas molecule cross-section (4.1×10^{-19} m^2 for oxygen) and n is the number of molecules per unit volume. At a pressure of 5×10^{-5} mm. Hg. we have

$$n = 6 \times 10^{23} \times \frac{10^3}{22.4} \times \frac{5 \times 10^{-5}}{760} = 1.8 \times 10^{18} \text{ molecules/cu. m.}$$

Substitution in the formula results in

$$\lambda = \frac{4}{4.1 \times 10^{-19} \times 1.8 \times 10^{18}} = 5.4 \text{ m.}$$

Since the electrons had to travel only a distance of some 1.5 m., no excessive scattering due to collisions with molecules was expected. This conclusion was borne out by the absence of an observable halo on the phosphor screen.

The earth's magnetic field was found to have a pronounced effect on the beam of ~ 10 kev electrons used in this experiment. Taking a value of 6×10^{-5} webers/m^2 for the earth's field, the radius of curvature of 10 kev electrons would be 5.6 m. This means that in a distance of 1.5 m. the electrons would deviate 20 cm. from their path. Since the evacuated tube was less than 8 cm. in diameter, shielding was obviously necessary. A sufficient quantity of transformer core metal in sheet form was provided free of charge by Canadian Westinghouse Co. This material served the shielding needs quite well.

(ii) Electron Source

The electron source is shown in fig. 6. A hot tungsten filament inside a cup held at high negative potential is the emitter of electrons. Five accelerating rings follow. Their potentials are linearly distributed between ground at the last ring and the high negative voltage at the filament. It was hoped that this arrangement might provide a sufficiently collimated beam for our purposes. Unfortunately, this was not the case and all measurements had to be made using baffles to simulate point sources rather than a broad parallel beam.

The accelerating rings and filament cup were held to the ground ring by means of four glass rods whose ends were threaded by means of a sand blast lathe. Glass sleeves were used as ring spacers. The ground ring in turn was attached to the end cap by means of four stainless steel rods. All metal parts of the source were made of stainless steel.

The electric circuit of the source is shown in fig. 7. The filament and accelerating rings were connected to glass-kovar terminals mounted in the end cap. Thus the 10 megohm voltage drop resistors could be mounted outside the vacuum system. A 12 volt car battery and rheostat in series were used to heat the tungsten filament.

Only electrons were used in evaluating the lens system. Ion sources are more difficult to construct and, since the equa-

tions of motion involved are the same, would provide no additional information about the focal properties of the lens system. In addition, the phosphor screen could not be used for very long as a target for a focused ion beam, since damage to the screen would soon render it useless for detection.

(iii) Lenses

Two identical lenses were employed in this experiment. Their construction is shown in fig. 8. The four poles were held inside a $1\frac{1}{2}$ inch diameter grounded cylinder by means of rubber-insulated screws. Flanges containing key-way slots were attached to the ends of the grounded cylinders. Thus the lenses could be moved to various positions on the central axis by means of the previously mentioned hollow rods. Each rod contained four leads connected to the lens poles through their mounting screws. The circuit used to control lens voltages is shown in fig. 9.

The lens poles were 2 inches long and 1/2 inch in diameter. As discussed in section A-1, the diameter can be 1.25 times the pole separation. Accordingly, the separation 2R was made 0.400 $\pm$ 0.002 inches.

In section A-1 it was also shown that the wave number is given by

$$k = \frac{1}{R}\sqrt{\frac{V_o}{V_s}} \qquad (10)$$

if relativistic effects are assumed to be negligible. Equation (10) applies when two lenses have voltage $+V_o$ and the other two, $-V_o$. Referring to fig. 9 it is apparent that in this experiment two poles were held at a positive voltage $+V_p$ and the other two poles were grounded. This was done purely as a matter of convenience. The equivalent k is obtained by replacing V_o in equation (10) with $V_p/2$. Thus

$$k = \frac{1}{0.200 \times 2.54} \sqrt{\frac{V_p}{2V_s}} = 1.39 \sqrt{\frac{V_p}{V_s}} \,. \qquad (30)$$

(iv) Voltage Measurements and Accuracy

The voltage on the lens poles, V_p, was measured with a "Sylvania" vacuum tube voltmeter (type 301), which has a manufacturers quoted accuracy of $\pm 3\%$. Accelerating voltages, V_s, were read on the indicator of the high voltage supply. Since these two voltages appear only as a ratio in all equations, a relative calibration of voltmeters was sufficient. The meters were compared using the high voltage scale on the vacuum tube voltmeter which had a full scale deflection of 5000 volts. It was assumed that the obtained calibration factor would be true up to 8000 volts, which was the highest value of V_s used in this experiment. The voltage supply meter was found to give readings 6.5% higher than the vacuum tube voltmeter. Consequently, this amount was added to all observed values of $\frac{V_p}{V_s}$.

All final values of V_p/V_s were arrived at by averaging five individual measurements with V_s set at 8, 7, 6, 5, and 8 thousand volts in turn. The probable error obtained from the standard deviation was less than 2% in all cases. However, it is possible to have a considerably larger systematic error. Since meter calibration and measurements of V_p were made on different scales of the vacuum tube voltmeter, the possible error in the voltage ratio is as high as $\pm 6\%$. The square root of this ratio would have a possible error of $\pm 3\%$. Combining this value

with the half percent uncertainty in the value of R , gives the total possible error for the wave number k , namely $\pm 3\frac{1}{2}\%$.

It remains to evaluate relativistic effects for the electron energies used in this experiment. The relativistic wave number k is defined in equation (10a) in terms of the quantity E which is given by

$$E = p\beta\frac{c}{2} \quad \text{(in electron volts)}.$$

From the total energy we have

$$p^2c^2 = eV_s\,(eV_s + 2m_oc^2)$$

$$= m_o^2c^4\left[x(x + 2)\right] ,$$

where $x = \dfrac{eV_s}{m_oc^2}$.

From the kinetic energy relationship we obtain

$$\beta^2 = \frac{x(x + 2)}{(x + 1)^2} .$$

Therefore,

$$E = \frac{1}{2}\,pc\beta$$

$$= \frac{m_oc^2}{2}\;\frac{x(x + 2)}{(x + 1)}$$

$$= eV_s\left[1 - \frac{x}{2(x + 1)}\right].$$

For an electron m_oc^2 = 511 kev and the highest energy used in this experiment was

$$eV_s = 8 \text{ kev.}$$

Thus we have $x = 0.0156$ and $E = eV_s\left[1-0.0077\right]$.

The quantity E differs only by 0.77% from the electron energy. Therefore the use of equation (10) instead of equation (10a) would give rise to an error of only 0.39% in the value of k. For lower values of V_s the error would be smaller still. Since the possible error introduced by voltmeter inaccuracy is considerably larger, the nonrelativistic equation (10) was considered sufficiently accurate.

2. Determination of Effective Lens Length.

As was previously stated, the effective length of a lens is not equal to the physical length of the pole-pieces, but is somewhat larger as indicated by equation (11). In this part of the experiment the effective length ℓ and the unknown factor f were determined. This was done by measurements of single lens focusing parameters and the application of equation (16), which gives ℓ as a function of a, b, and k . If the last three variables could be accurately determined, it would be a simple matter to calculate ℓ . This, however, is not quite the case. First of all, for a given physical arrangement of source, lens and image plane, the values of effective a and b will depend on the value of ℓ . Secondly, there was some uncertainty as to the exact position of the electron point source. Thus the value of a was not accurately known even as a function of ℓ .

To get around this difficulty use was made of the fact that the effective length should remain unchanged as the lens is moved to various positions. This will be true for the calculated ℓ only when correct values are used for both a and b . If the assumed source position is incorrect, the calculated ℓ will vary as the lens is moved.

The physical arrangement is shown in fig. 10. Two baffles, made by piercing thin metal foil, were used to simulate a point source and to limit the width of the beam. The first baffle had an aperture of about $\frac{1}{4}$mm. and acted to produce a point source. The second baffle (16 cm. removed) had an aperture of 1 mm. dia., which insured that the beam would not be much wider than 3 mm. at the maximum object distance used (about 50 cm.).

The effective source position is shown at some distance u from the first baffle. This uncertainty in position is a result of finite first aperture diameter. Distances a_o and b_o were measured from the center of the lens to the first baffle and to the phosphor screen, respectively. The screen was 154.0 cm. away from the first baffle. With these definitions it is obvious that

$$\left.\begin{aligned} a &= a_o + u - \ell/2 \ , \\ b &= b_o - \ell/2 \ , \\ a_o &+ b_o = 154.0 \text{ cm.} \end{aligned}\right\} \qquad (31)$$

and

Substitution of expressions (31) in equation (16) yields

$$\tan k\ell = \frac{k(154.0 + u - \ell)}{k^2(a_o+u-\ell/2)\ (154.0-a_o-\ell/2) - 1} \ . \qquad (32)$$

The experimental values of k obtained for various lens positions are listed in Table 1. Each of the two lenses was used for half the total measurements. The lens which was always placed closest to the source in the two lens experiment is called number one. When lens voltages were adjusted to the focused condition, a line less than 1 mm. thick was observed on the phosphor screen in every case.

TABLE I.

Single Lens Observations

Lens Number	a_o, cm.	k, $cm.^{-1}$
1	16.9	0.1048
1	23.0	0.0942
2	27.0	0.0881
1	31.0	0.0846
2	35.0	0.0811
1	39.0	0.0789
2	43.0	0.0756
2	51.0	0.0725

TABLE II.

Calculated Single Lens Results

a_o, cm.	Calculated ℓ, cm.			
	u = 0	u = 2cm.	u = 3cm.	u = 4cm.
16.9	6.52	5.81	5.53	5.27
23.0	6.08	5.61	5.43	5.24
27.0	6.07	5.67	5.51	5.35
31.0	5.87	5.56	5.41	5.28
35.0	5.84	5.56	5.45	5.33
39.0	5.69	5.48	5.38	5.26
43.0	5.82	5.63	5.53	5.44
51.0	5.74	5.58	5.52	5.44

Values from Table I were used in equation (32) to calculate the effective length ℓ for $u = 0$, 2, 3 and 4 cm. Calculations were carried out graphically and the results are given in Table II. The calculated values of ℓ were also plotted in fig. 11. It is seen that for $u = 0$ and $u = 2$ cm. the calculated ℓ increases with decreasing a_o. When $u = 4$ cm., the value of ℓ decreases with decreasing a_o. The in-between position of $u = 3$ cm. gives an ℓ relatively independent of a_o. Thus in the following narrow beam, two lens experiment it was assumed that the point source is located 3 cm. from the first baffle (towards the accelerator).

The average value of ℓ for $u = 3$ cm. was found to be 5.47 cm. According to equation (11) we thus have

$$f = \frac{5.47 - 5.08}{1.016} = 0.38 \quad .$$

Examination of equation (16) will reveal that ℓ is proportional to $1/k^2$ when $k\ell \ll 1$ and $k^2ab \gg 1$. These conditions were approximately satisfied in this experiment. Consequently, the possible error in ℓ is about $\pm 7\%$ (twice the possible error in k). This results in

$$\ell = 5.47 \pm 0.38 \text{ cm.} \qquad (33)$$

and

$$f = 0.38 \pm 0.37 \quad . \qquad (34)$$

Although the indicated possible error in f is almost 100%, the actual error is probably considerably smaller. I.E. Dayton et al. (4) quote a measured value of 0.57 for a magnetic lens and C.F. Giese (7) gives a value of 0.249 for an electrostatic lens.

3. Narrow Beam Focusing With Two Lenses

In this section the results of focusing a point source to a point image on the phosphor screen are reported. The effective point source simulation was achieved with the same baffle set-up as in the previous section. It was assumed that the point was 3 cm. behind the first baffle and that ℓ = 5.47 cm. Thus the effective values of s/ℓ, a/ℓ and b/ℓ could be readily calculated for any lens placements. Various combinations of these three variables are given in the first three columns of Table III. Columns 4 and 5 list the corresponding focal strengths, calculated with the aid of the nomograph of fig. 4. Focal strengths obtained from measurements are given together with their percent differences from calculated values in columns 6 and 7. The results are also represented graphically in figs. 12 and 13. Cross-marks indicate measured points and the solid lines represent best smooth curves drawn through the calculated points.

In general the agreement between measured and calculated values is quite good. More than half the errors are 0.5% or less and none exceed 3.5% which is the possible error in k. The biggest errors occur in $k_2\ell$ at the largest lens separation, s/ℓ = 2.95. Generally, the measured values of $k_1\ell$ have a tendency to be high and measured $k_2\ell$ tend to be low. It is difficult to force any conclusions from these slight trends in errors. The measurements were of necessity somewhat subjective, since the experimenter had to judge at what lens voltage settings optimum focusing was achieved. However, the observed final image point was quite small. In all cases it was less than 1 mm. in both dimensions.

TABLE III

Narrow Beam Two Lens Results

s/ℓ	a/ℓ	b/ℓ	Calculated focal strengths		Measured focal strengths			
			$k_1\ell$	$k_2\ell$	$k_1\ell$	Error	$k_2\ell$	Error
0.481	3.14	23.1	.802	.691	.815	1.6%	.694	.4%
"	4.96	21.3	.716	.656	.720	.6%	.654	.3%
"	6.43	19.8	.675	.634	.676	.2%	.632	.3%
"	7.90	18.3	.650	.622	.647	.5%	.615	1.1%
"	3.87	22.4	.757	.674	.768	1.5%	.676	.3%
0.975	3.19	22.6	.748	.624	.759	1.5%	.626	.3%
"	4.48	21.3	.682	.600	.685	.4%	.599	.2%
"	5.94	19.8	.637	.584	.643	.9%	.581	.5%
"	7.40	18.3	.608	.572	.610	.3%	.566	1.1%
"	6.67	19.1	.621	.576	.624	.5%	.575	.2%
"	5.21	20.5	.653	.590	.660	1.1%	.588	.3%
"	3.74	22.0	.715	.614	.723	1.1%	.614	0%
1.96	3.30	21.4	.687	.544	.692	.7%	.540	.7%
"	4.22	20.5	.639	.533	.642	.5%	.531	.4%
"	4.95	19.8	.610	.525	.618	1.3%	.523	.4%
"	5.68	19.1	.589	.519	.591	.3%	.512	1.4%
"	6.41	18.3	.573	.515	.575	.4%	.510	1.0%
2.95	3.23	20.5	.669	.498	.671	.3%	.490	1.6%
"	3.96	19.8	.620	.491	.625	.8%	.482	1.8%
"	4.70	19.1	.593	.486	.591	.3%	.471	3.1%
"	5.43	18.3	.562	.479	.565	.5%	.468	2.4%

4. Wide Beam Focusing

This part of the experiment is concerned with finding the dependence of effective focal strength on radial distance within the lens. Direct measurements of focal strengths were obtained for electrons entering the lenses at various distances from the central axis.

The arrangement shown in fig. 14 was used. Both lenses were placed in fixed positions near the phosphor screen. One baffle with an aperture approximately 1 mm. wide was placed 113.5 cm. in front of the first lens. The second baffle, placed 3.1 cm. in front of the first lens, contained four holes, each about 0.5 mm. in diameter. The holes were positioned at the extremities of an imaginary vertical cross with both members d mm. long. Thus four nearly parallel pencils of electrons were produced. Their separation was varied by using baffles having different values of d.

With all lens poles set at ground potential, four distinct points were visible on the phosphor screen. The points were no bigger than 1 mm. in diameter. When focusing voltages were gradually applied, the points converged to a line (single lens focusing) or to a point (two lens focusing). At the optimum condition in two lens focusing the centers of individual points were within 1 mm. of each other.

For the same reasons as found in previous sections, the effective point source was not expected to coincide with the first baffle. However, this time the length ℓ and image distance b are both known. Thus a measurement of k will determine the effective

object distance through the single lens formula (16). Measured values of $k\ell$ are given for both lenses in Table IV. Note that as d increases from 2 to 8 mm., the average increase in measured $k\ell$ is about 1%. This effect can be interpreted in three possible ways. It may be assumed that the effective $k\ell$ drops with increasing radial displacement within the lens. On the other hand, it may be construed that the effective source position approaches the lenses as d is increased. A third plausible interpretation would be to combine the first two assumptions.

Columns 3 and 5 (in Table IV) give the calculated distances between the source and the first lens. The value a, given in column 6, represents the average distance calculated from both lenses. If the variation in $k\ell$ is due to lens fringe effects, then the best source position is given by d = 2 mm., i.e. a = 165 cm. From geometrical considerations it is obvious that for this source position the baffles would leave no open straight line paths when d = 4, 6 and 8 mm. It is therefore considered very likely that the source position did vary. The calculated positions for d = 6 and 8 mm. are still too far away to be geometrically possible. Thus the only logical explanation would be to assume the effective strength of the lens actually increases with increasing radial distance. This would make the calculated values of a appear too large.

Let us take an extreme case and assume that for d = 8 mm. the source position coincides with the first baffle (a = 113.5 cm.). Then we can calculate $k\ell$ from equation (16), which yields

$$k\ell = 0.450 \quad \text{for the first lens,}$$

and

$$k\ell = 0.517 \quad \text{for the second lens.}$$

The average difference between these figures and the measured values (Table IV) is 2%. It is therefore concluded that, for radial displacements up to about 0.8R, the effective focal strength probably remains within 2% of its value at the center.

TABLE IV

Wide Beam Single Lens Results

d	First lens		Second lens		Average a, $\frac{a_1 + a_2}{2}$ cm.
mm.	$k\ell$	a_1, cm.	$k\ell$	a_2, cm	
2	0.433	168	0.505	161	165
4	0.434	165	0.506	153	159
6	0.434	165	0.509	142	154
8	0.436	155	0.512	130	142

Measurements were also made for two lens focusing. Readings could not be obtained for d = 8 mm., since two points would disappear from the image when focusing was attempted. Apparently, divergence inside the first lens was sufficient to cause collision with the poles of the second lens. Results are given in Table V. The calculated strengths were obtained using $b/\ell = 4.19$, $s/\ell = 0.975$ and the average values of a/ℓ derived from Table IV. The measured values disagree from calculated ones by less than 1%.

TABLE V

Wide Beam Two Lens Results

d, mm.	average a/ℓ	Calculated focal Strengths		Measured focal strengths			
		$k_1\ell$	$k_2\ell$	$k_1\ell$	Error	$k_2\ell$	Error
2	30.1	.593	.689	.592	.2%	.688	.2%
4	29.1	.594	.689	.593	.2%	.683	.9%
6	28.1	.595	.690	.594	.2%	.689	.2%

D. SUMMARY AND CONCLUSIONS

A single quadrupole lens can converge an ion (or electron) beam in one plane and diverge it in the other plane. With two lenses convergence can result in both planes, regardless of lens positions. In fact, a real point image can always be obtained from a point object when proper focal strengths are used. This is also true for a parallel beam source (point object at infinite distance).

A successful method for finding the effective length of a lens was presented in section C-2. This length is larger than the physical length of poles due to the presence of fringe fields at the ends. The lenses used in this experiment (see fig. 8) had a physical length of 2 inches or 5.08 cm. Their measured effective length was 5.47 cm. with a possible error of 0.38 cm. The method for finding effective lens length also provides a measure of the point object position. This information was necessary for later experiments involving two lenses.

A considerable number of measurements were carried out with the two lens system. The nomograph, designed for easing numerical computation, was used to calculate theoretical focal strengths. These were found to be in good agreement with the measured values.

Measurements of lens properties at various distances from the central axis show very little variation. Higher experimental accuracy than was achieved would be required if definite conclusions were to be drawn. However, results tend to indicate that the effective focal strength increases with radial displacement but does not

exceed a 2% increase up to a distance of 0.8R.

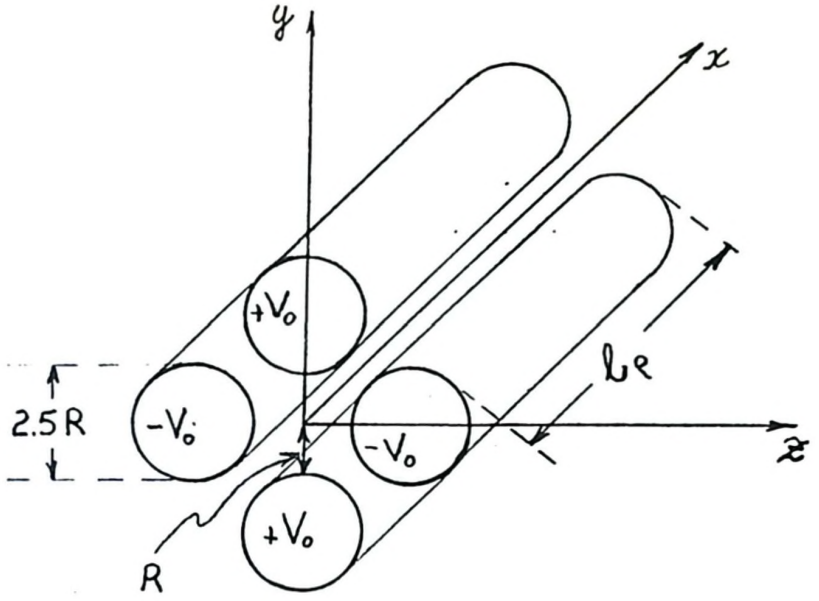

FIGURE 1.

QUADRUPOLE LENS.

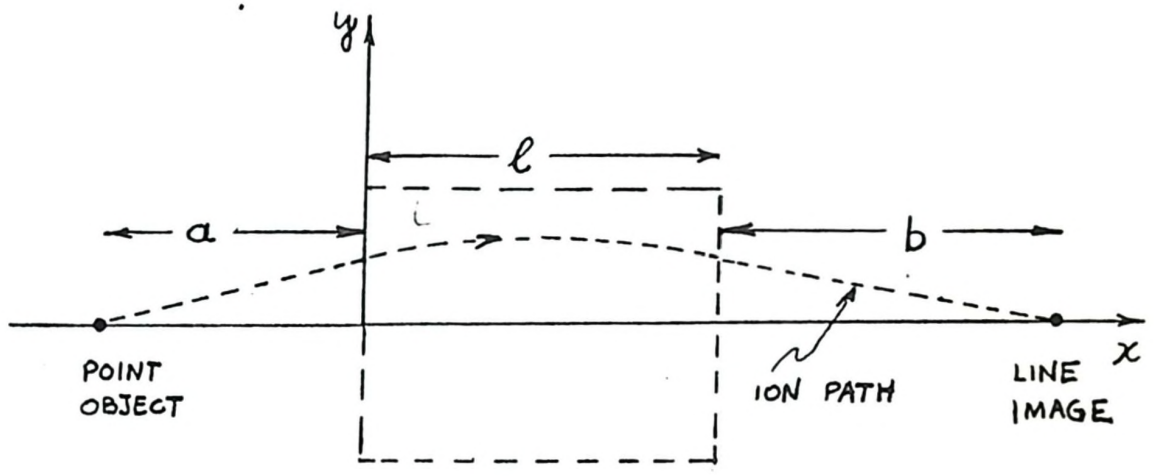

FIGURE 2.

SINGLE LENS FOCUSING.

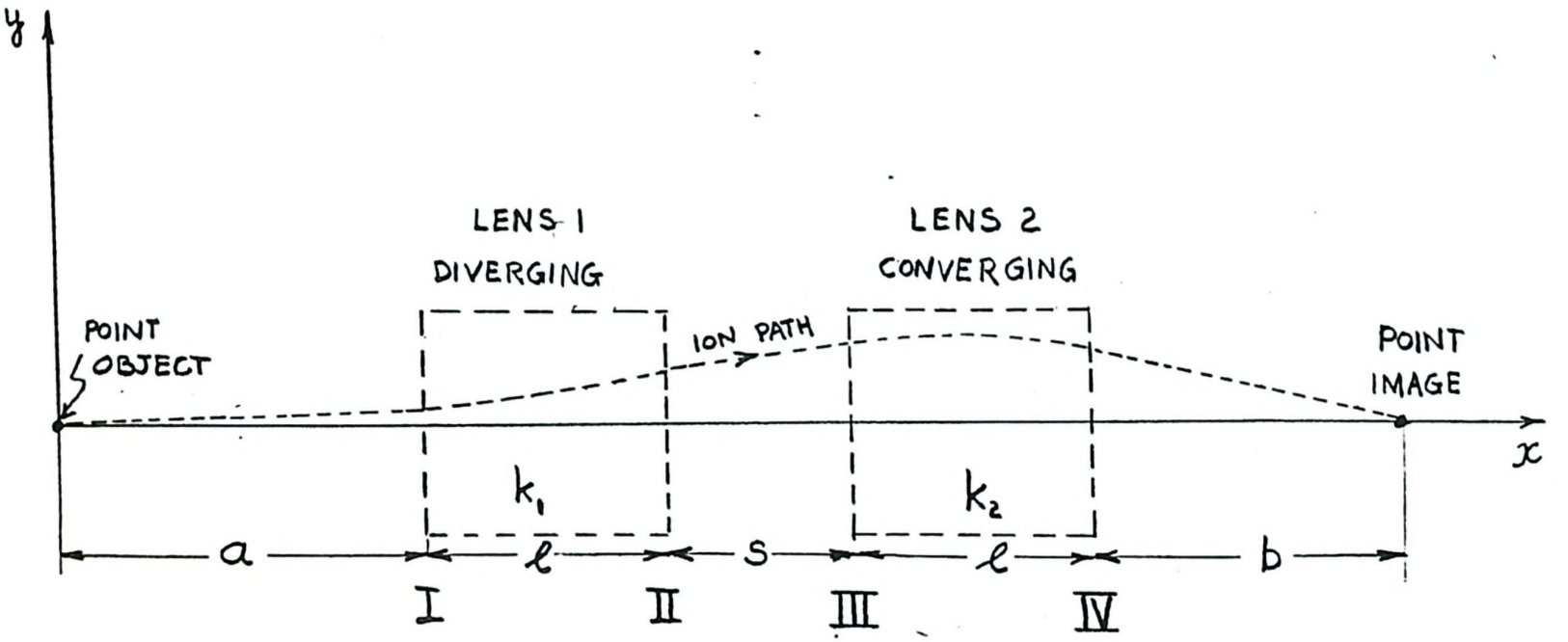

FIGURE 3.

TWO LENS FOCUSING.

FIGURE 4.

NOMOGRAPH FOR THE TWO LENS SOLUTION.

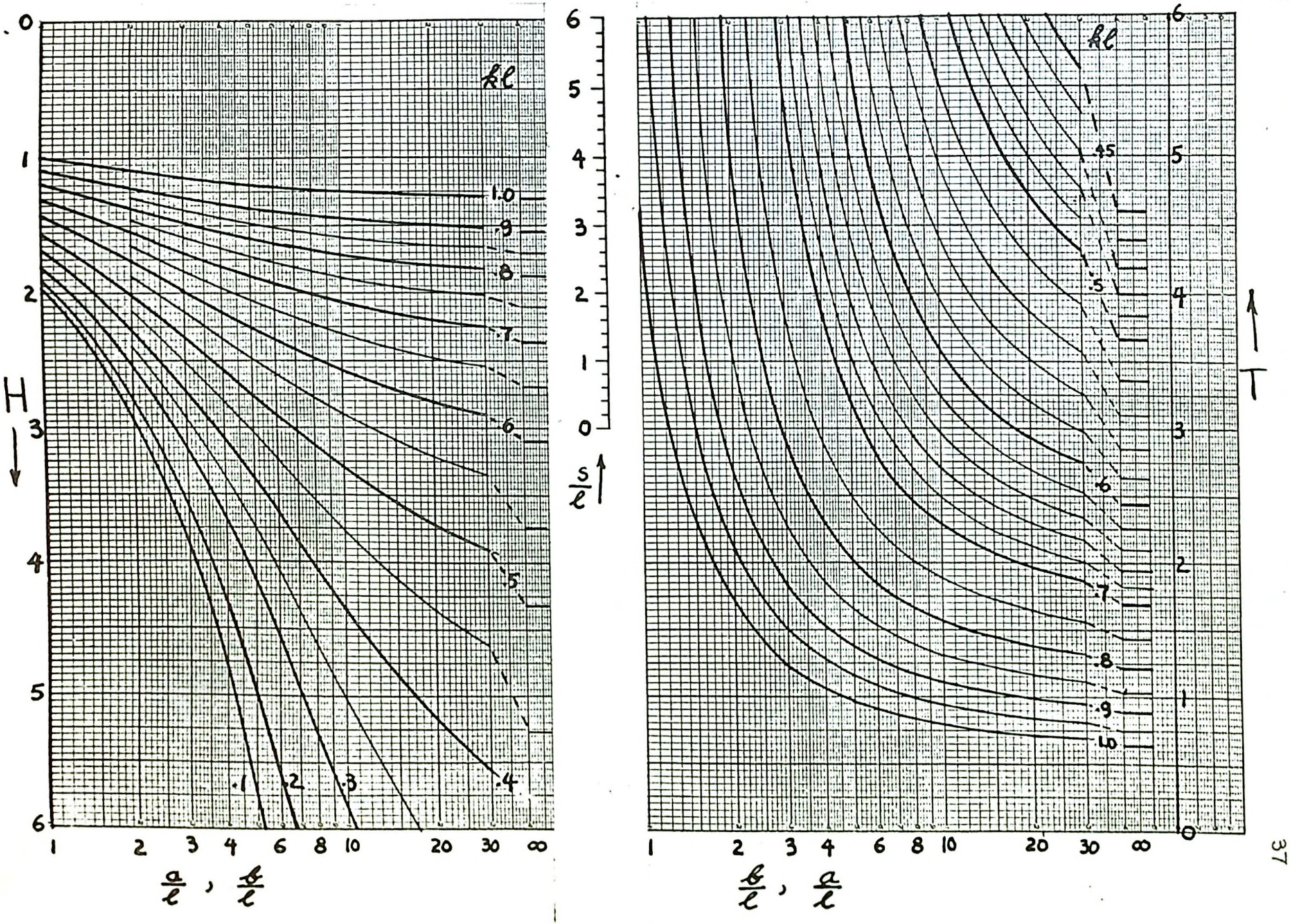

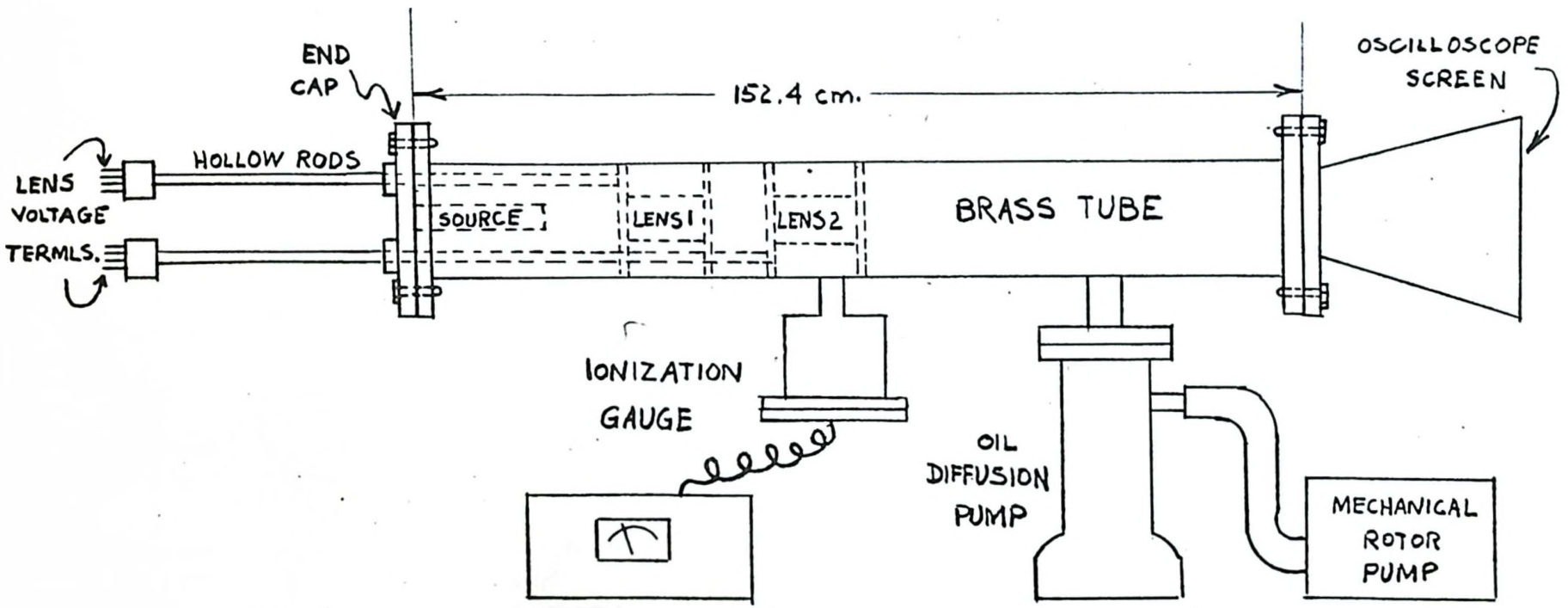

FIGURE 5.

SCHEMATIC DIAGRAM OF EXPERIMENT.

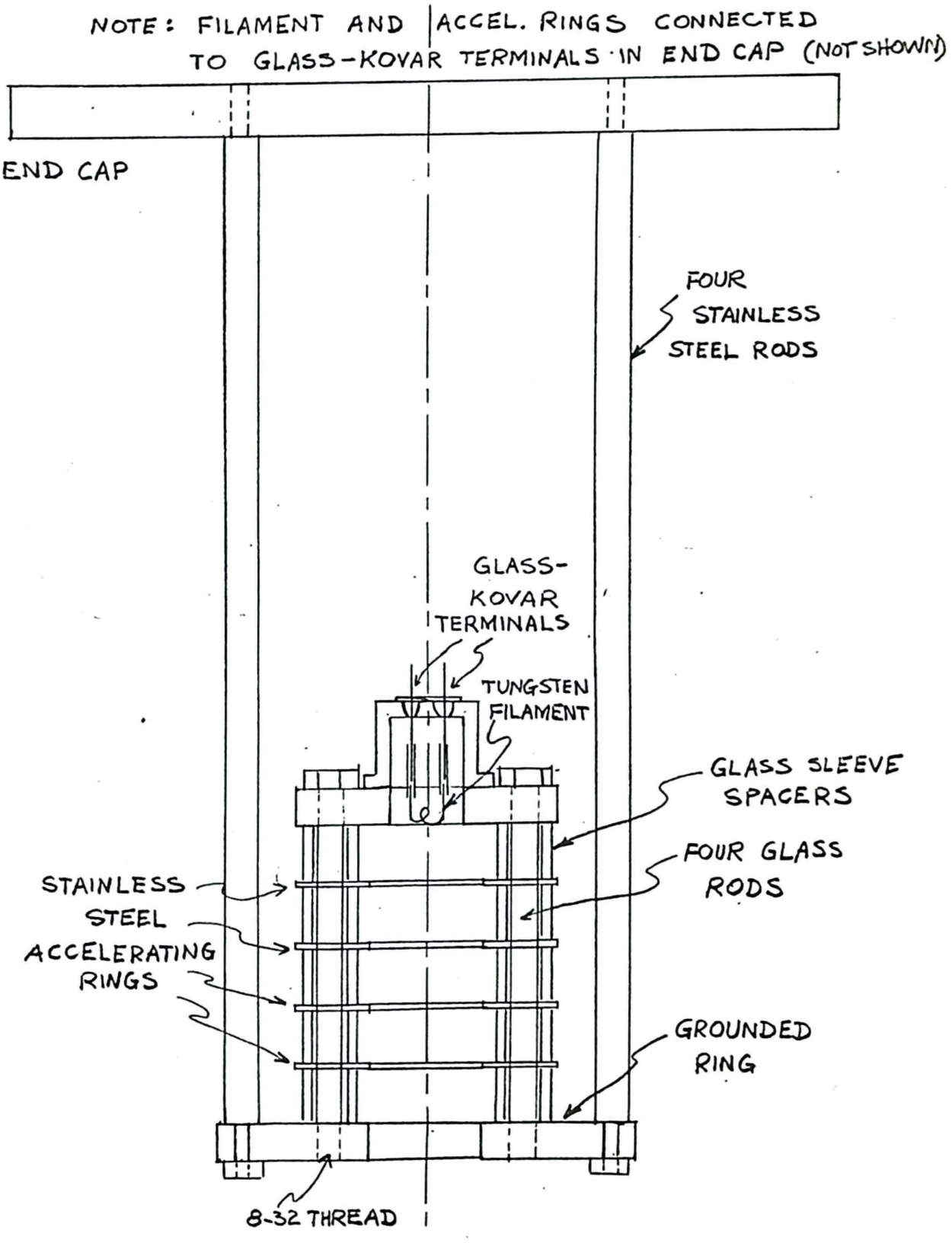

FIGURE 6.

CROSS SECTION OF ELECTRON SOURCE.
SCALE 1:1

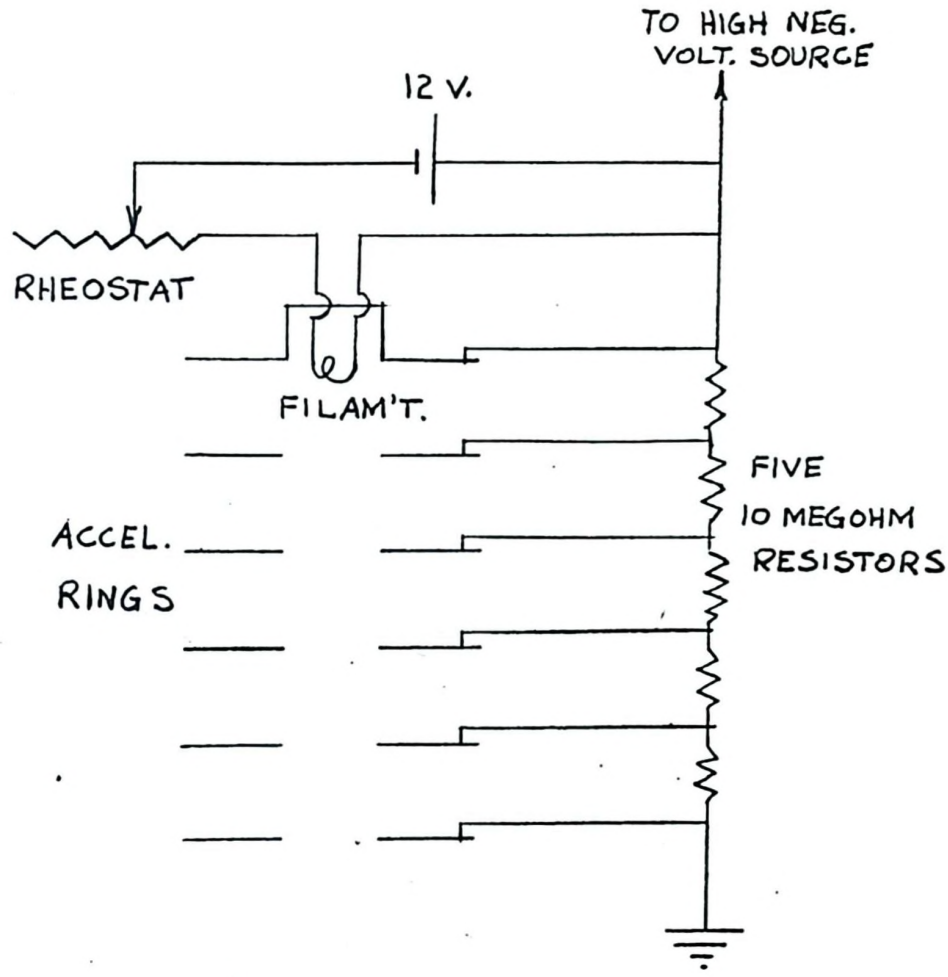

FIGURE 7.

ELECTRON SOURCE
CIRCUIT.

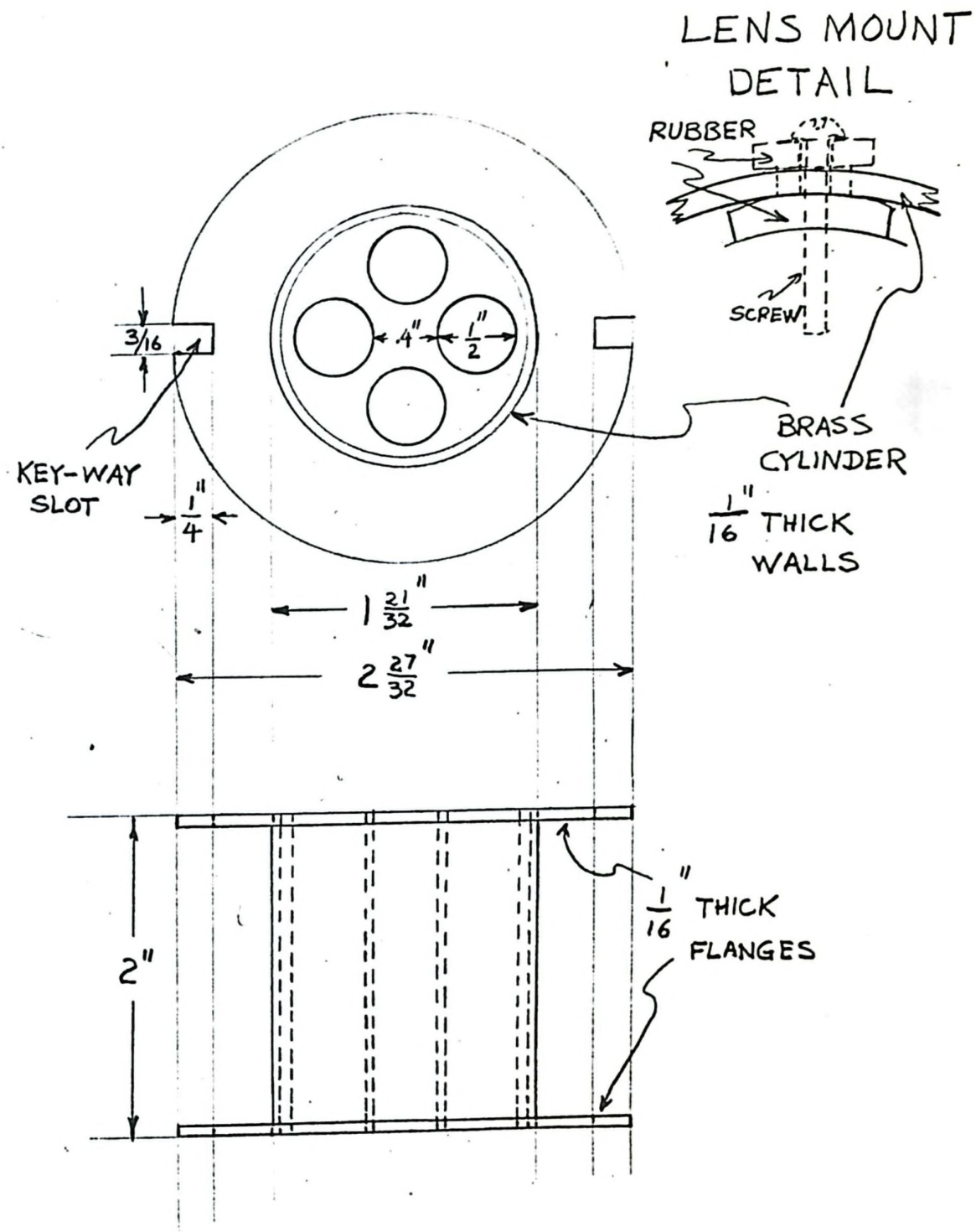

FIGURE 8.

LENS USED IN EXPERIMENT.

SCALE 1:1

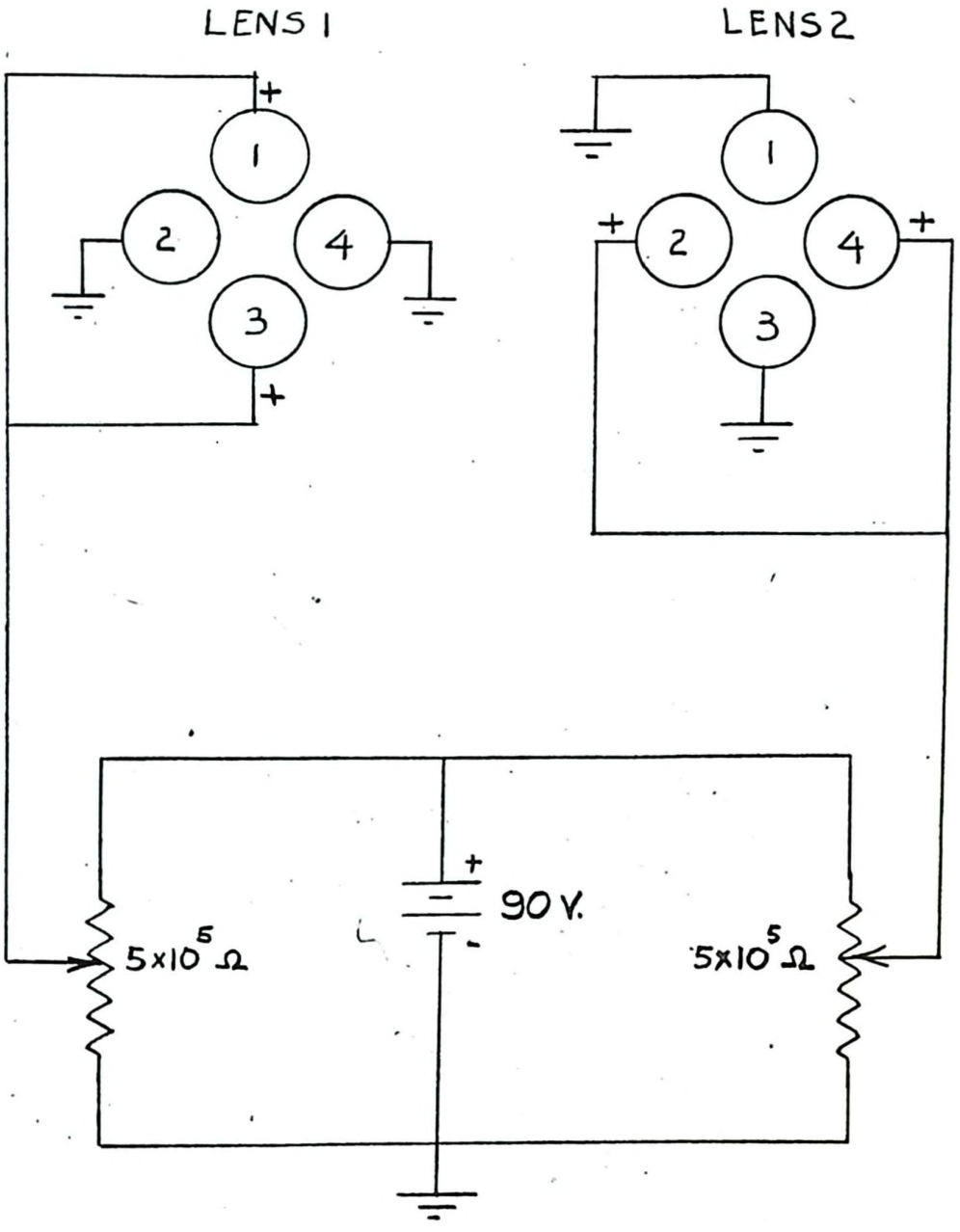

FIGURE 9.

LENS CONTROL CIRCUIT.

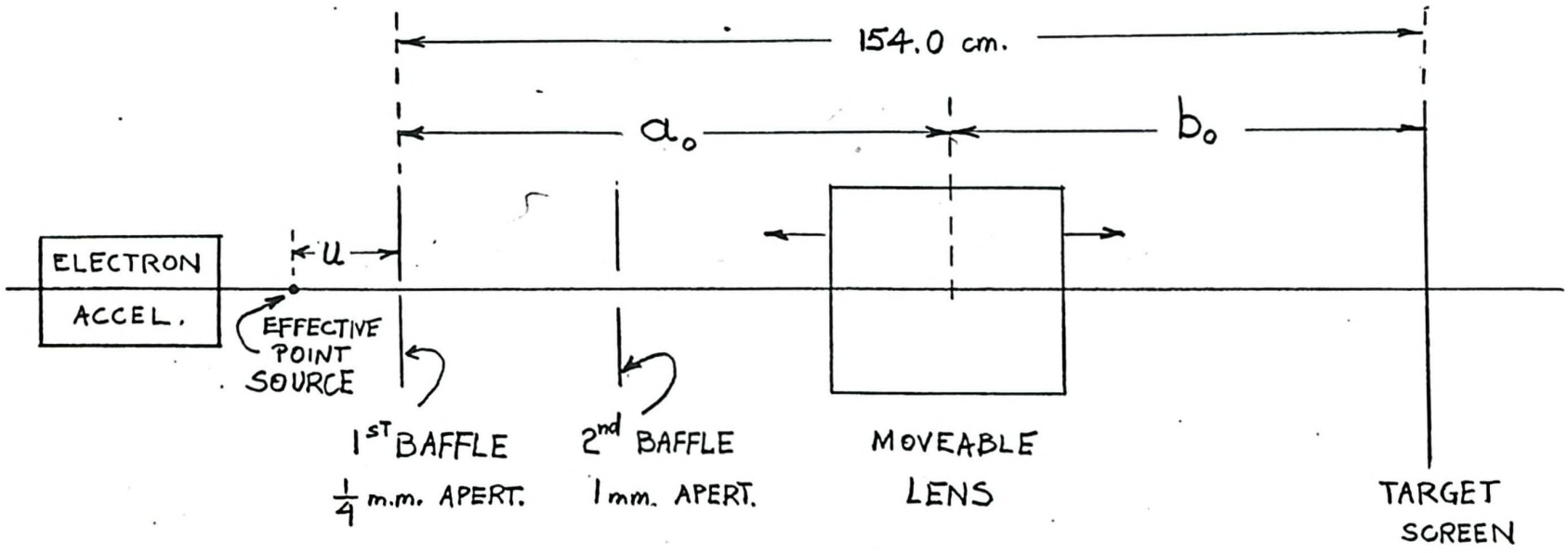

FIGURE 10.

SINGLE LENS EXPERIMENT.

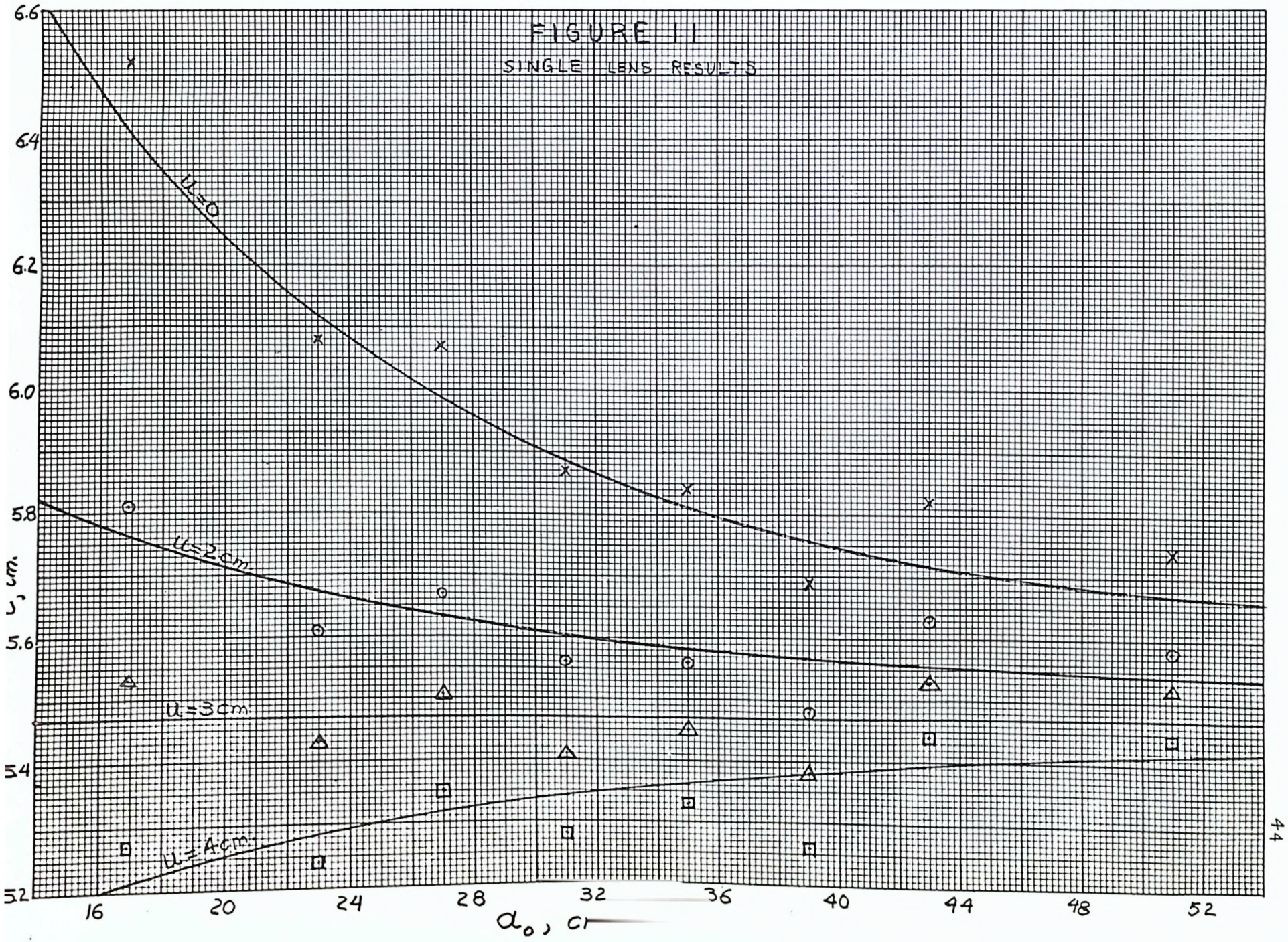
FIGURE 11
SINGLE LENS RESULTS
6.6
6.4
6.2
6.0
5.8
5.6
5.4
5.2
u=0
u=2cm.
u=3cm.
u=4cm.
16
20
24
28
32
36
40
44
48
52
d_o, cm

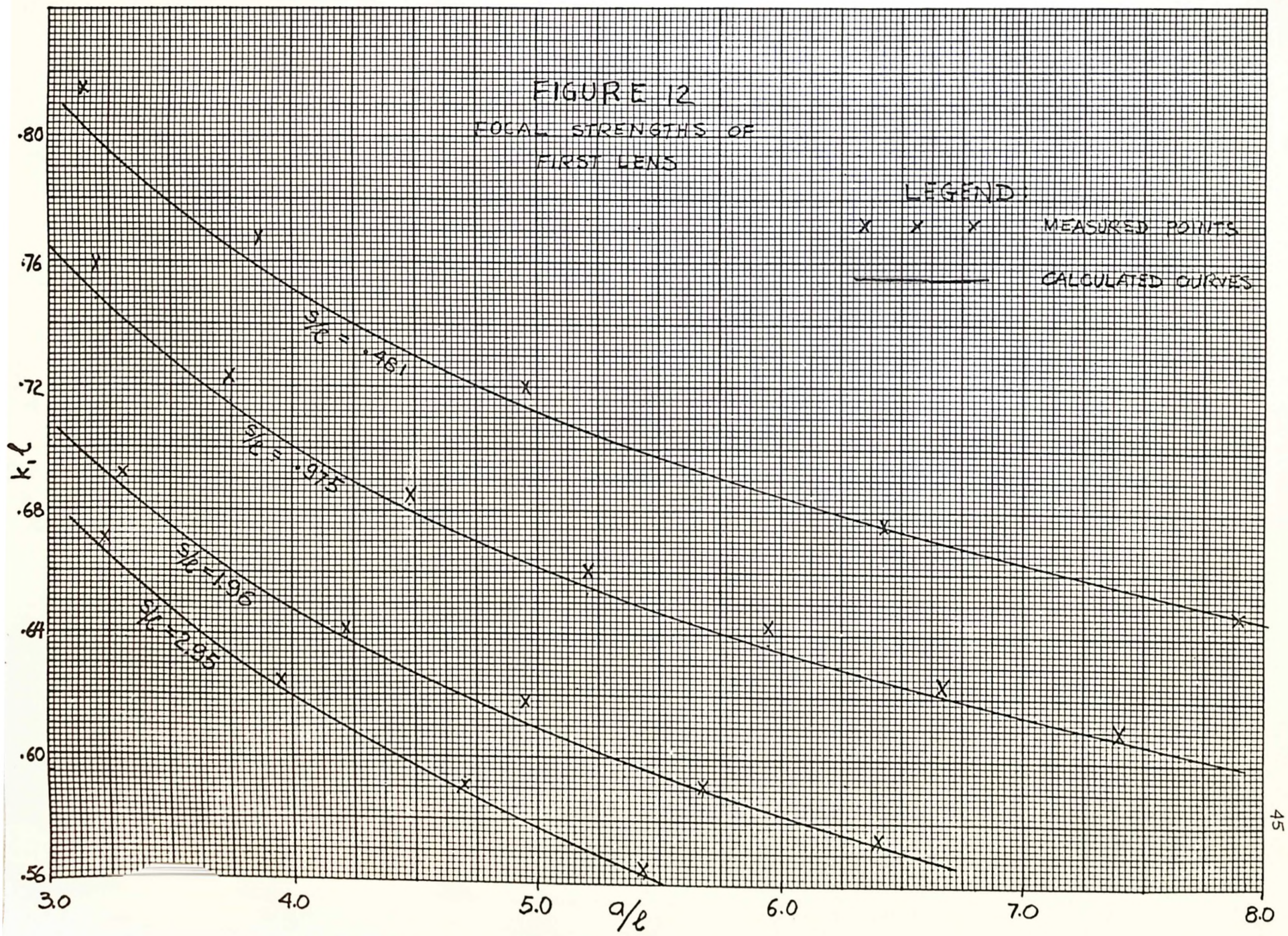
FIGURE 12
FOCAL STRENGTHS OF
FIRST LENS
LEGEND:
MEASURED POINTS
CALCULATED CURVES
s/c = .461
s/c = .975
s/c = 1.976
s/c = 2.95
k, ℓ
.80
.76
.72
.68
.64
.60
.56
3.0
4.0
5.0
6.0
7.0
8.0
a/ℓ

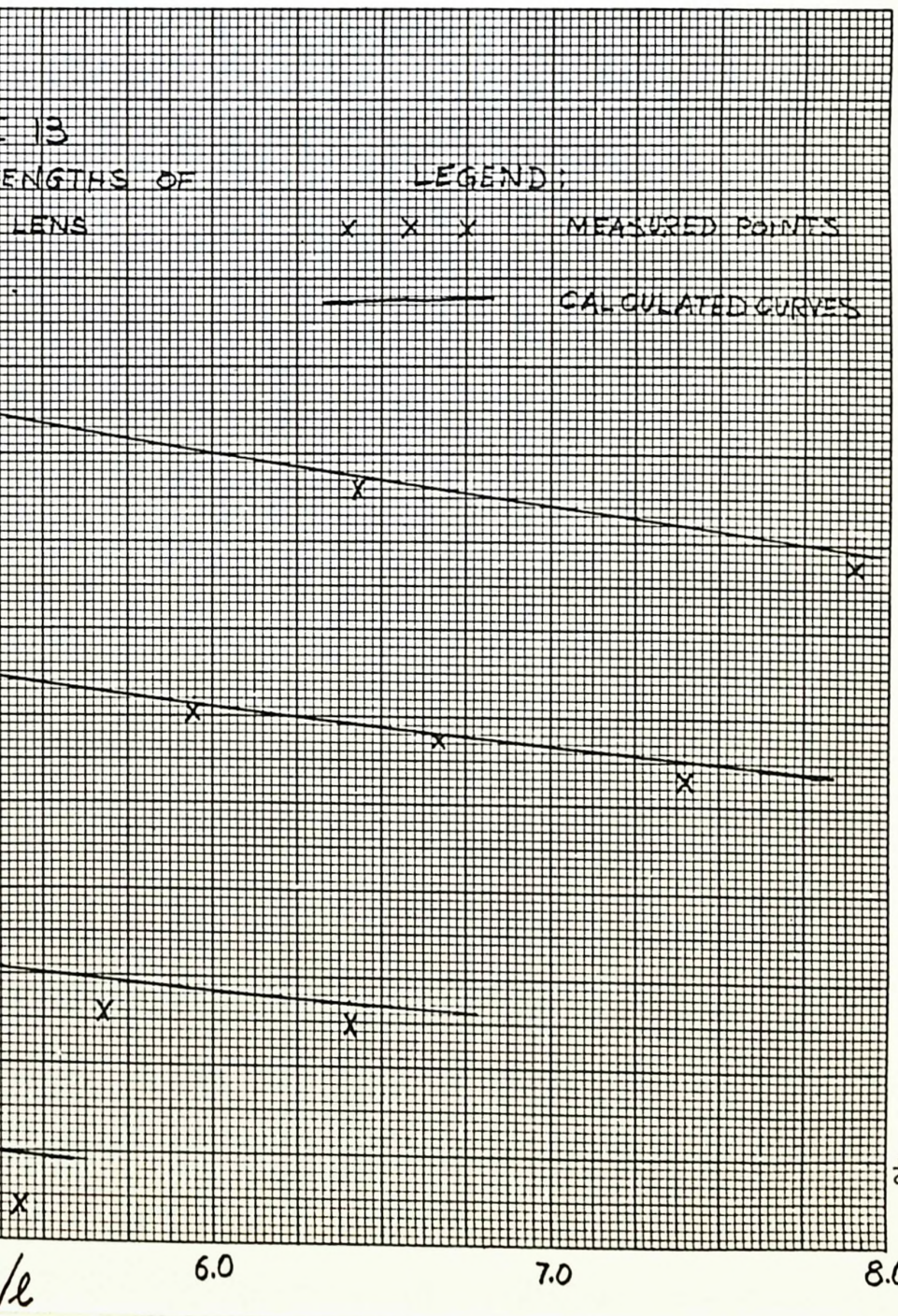
13
ENGTHS OF
LENS
LEGEND:
MEASURED POINTES
CALCULATED CURVES
6.0
7.0
8.0
/l

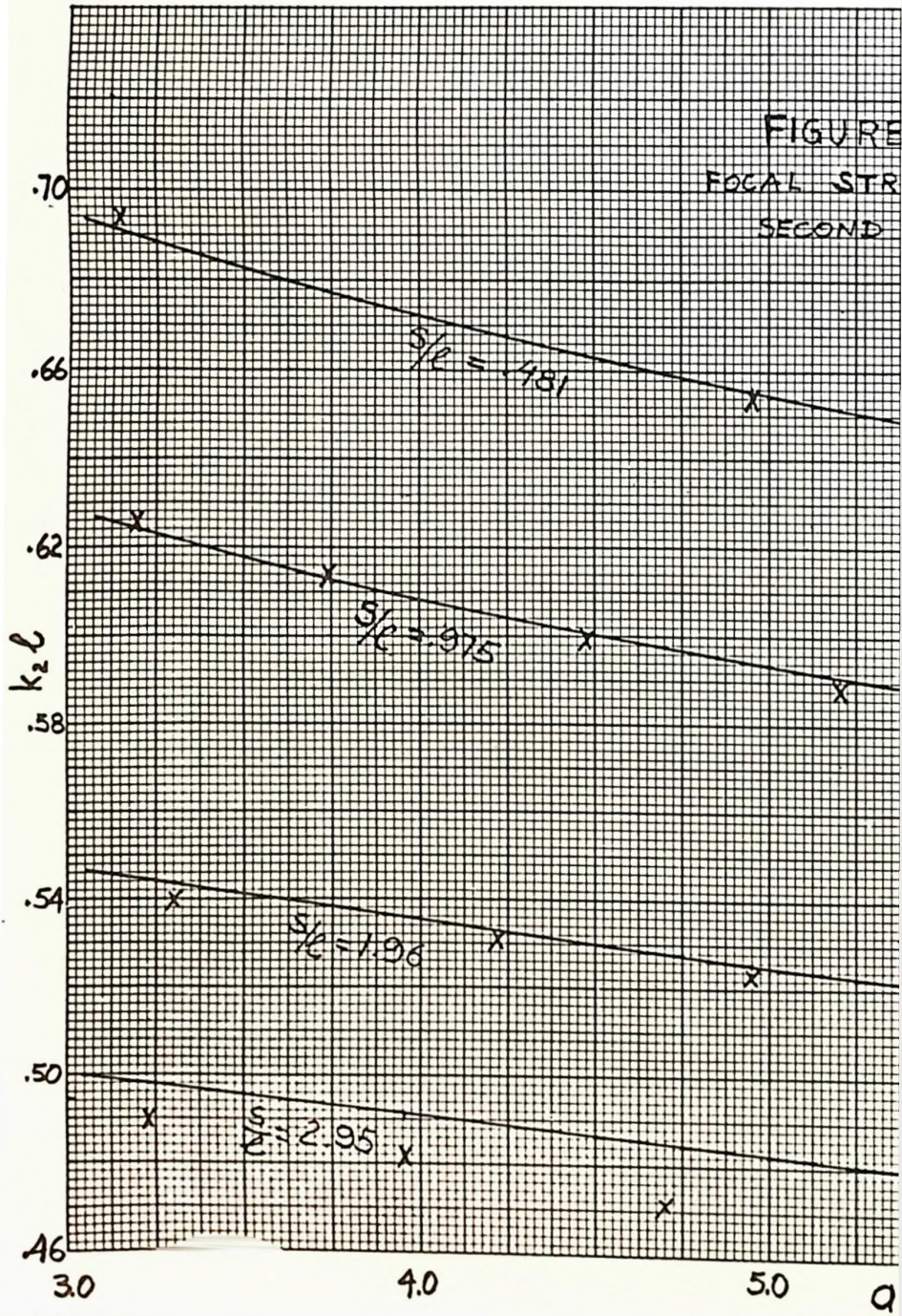
FIGURE
FOCAL STR
SECOND
.70
.66
.62
.58
.54
.50
.46
$k_2 l$
$S/l = .481$
$S/l = .975$
$S/l = 1.96$
$S/l = 2.95$
3.0
4.0
5.0

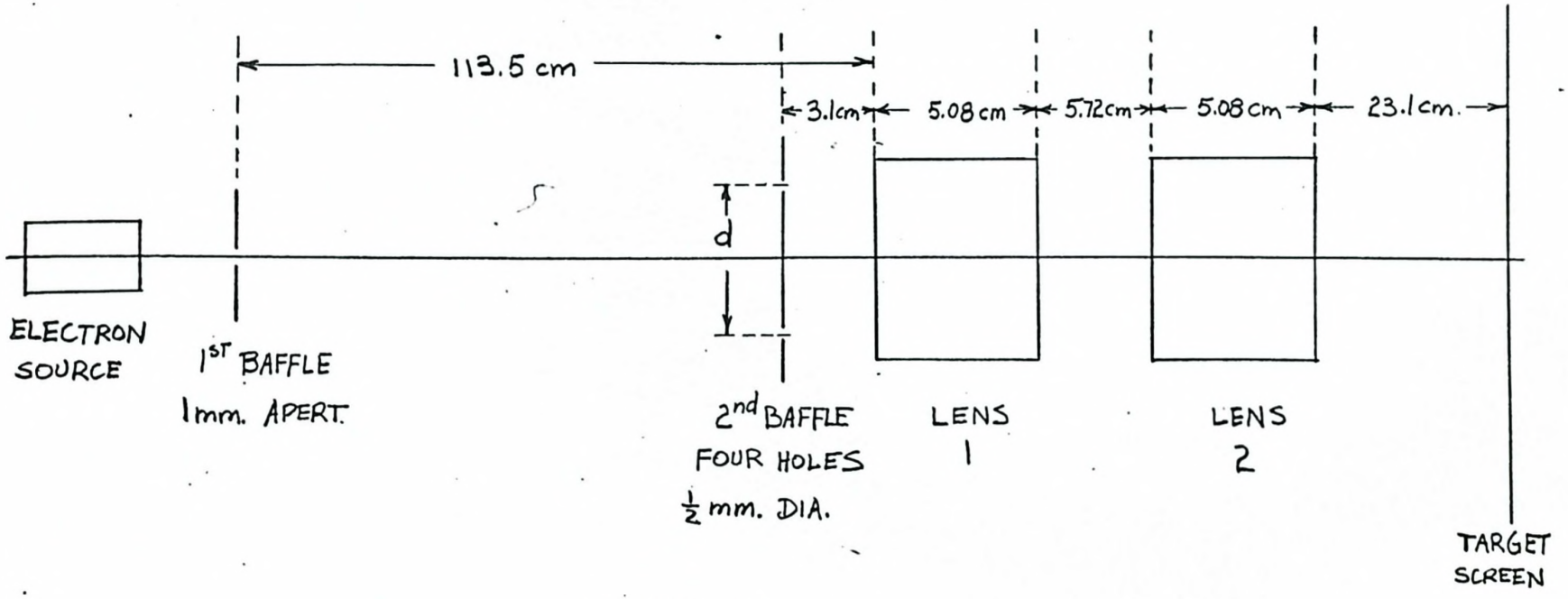

FIGURE 14.

WIDE BEAM EXPERIMENT.

(NOT TO SCALE)

BIBLIOGRAPHY

(1) Courant, Livingston and Snyder, Phys. Rev., 88, 1190 (1952)

(2) Blewlett, J. P., Phys. Rev., 88, 1197 (1952).

(3) Elmore, W. C. and Garret, M. W., Rev. Sci. Instr., 25, 480 (1954).

(4) Dayton, Shoemaker and Mozley, Rev. Sci. Instr., 25 485 (1954).

(5) Enge, H. A., Rev. Sci. Instr., 29, 885 (1958).

(6) Enge, H. A., Rev. Sci. Instr., 30, 248 (1959).

(7) Giese, C. F., Rev. Sci. Instr., 30, 260 (1959).

(8) Shull, MacFarland and Bretscher, Rev. Sci. Instr., 25, 364 (1954).

(9) Sears, F. W., Thermodynamics, p. 258, Addison-Wesley Publ. Co. (1953).